Growth-rate dependence of the structural transition of bismuth islands on Si(111) substrates

Ryota Ushioda,[1] Maimi Shimura,[1] Kan Nakatsuji,[2] and Hiroyuki Hirayama [1,*]
[1]Department of Physics, Tokyo Institute of Technology, J1-3, 4259 Nagatsuda, Midori-ku, Yokohama 226-8502, Japan
[2]Department of Materials Science and Engineering, Tokyo Institute of Technology, J1-3, 4259 Nagatsuda, Midori-ku, Yokohama 226-8502, Japan

(Received 21 June 2021; revised 31 January 2022; accepted 29 March 2022; published 15 April 2022)

During the growth of ultrathin Bi films, Bi(110) islands with a black phosphorus (BP)-like structure nucleate initially. These Bi(110) islands reorganize to Bi(111) islands with a rhombohedral structure at a certain critical thickness θ_c. This transition has been theoretically explained by the balance between the surface and bulk energies of the Bi islands with the two structures. However, we found that θ_c decreases with increasing growth rate on both Si(111)$\sqrt{3} \times \sqrt{3}$-B and 7×7 substrates according to the results of scanning tunneling microscopy observations. Monte Carlo simulations revealed that the edges of the Bi(110) islands become rough at higher growth rates. These rough edges effectively capture migrating atoms injected at the gaps and tops of the preexisting Bi(110) islands, thereby suppressing further Bi nucleation on the Bi(110) islands and promoting the lateral expansion of the islands while maintaining the original height. However, the strain cannot be relaxed effectively by edges in the laterally extended Bi(110) islands. Thus θ_c is considered to decrease in growth at larger rates.

DOI: 10.1103/PhysRevMaterials.6.043403

I. INTRODUCTION

Bismuth (Bi) is the heaviest nonradioactive element with an atomic number of 83. Owing to its large spin-orbit interaction, Bi has been considered as a key element for two-dimensional topological insulators. Indeed, Bi films were theoretically predicted to be two-dimensional topological insulators in their ultrathin limit [1,2]. In particular, the growth of Bi films on Si substrates is of great interest with respect to realizing Si-compatible spintronic applications.

Bi adopts a rhombohedral structure in bulk. In contrast, Bi(110) islands with a black phosphorus (BP)-like allotrope structure were observed to nucleate in the initial stage of growth on various substrates [3–20]. In the BP-like structure, each Bi atom uses all three of its covalent bonds to form paired layers. Thus energetically unfavorable dangling bonds are not present at the surface of the BP-like Bi(110) islands [Fig. 1(a)]. The surface term makes a more dominant contribution to the formation energy than the bulk term in nanoscale islands [21]. Thus Bi nanoislands preferentially adopt the BP-like Bi(110) structure during the initial stage of growth, despite the higher strain compared with the rhombohedral structure. In the BP-like Bi(110) islands, the paired layers stack along the surface normal orientation by van der Waals interactions, as illustrated in Fig. 1(a). Therefore these islands possess heights of multiples of bilayers (BLs) [3,20].

However, the relative contributions of the surface and bulk to the formation energy become inverted as the volume of the islands increases [21], which triggers a phase transition from the BP-like Bi(110) islands to rhombohedral Bi(111) islands beyond a certain critical thickness θ_c. This transition was experimentally observed to occur at $\theta_c = 6$ ML during the growth of Bi islands on the Si(111)7×7 substrate [3,20]. Theoretical calculations also supported that the transition occurs at $\theta_c = 6$ ML irrespective of the Bi/substrate interface structure [3]. However, we found that the transition did not take place even at $\theta = 60$ ML during the growth of Bi on the Si(111)$\sqrt{3} \times \sqrt{3}$-B substrate [7], despite the fact that it would be expected to occur at $\theta_c = 6$ ML with respect to the energetics. The Bi film growth was conducted at a rate of 0.035 ML/min on the Si(111)$\sqrt{3} \times \sqrt{3}$-B substrate [7], whereas it was conducted at 0.43 ML/min on the Si(111)7×7 substrate [3]. This suggested that θ_c may be strongly influenced by kinetic processes during island growth. Thus, in this study, we examined the influence of the growth rate on the nucleation and growth of Bi islands and their subsequent structural transition on the Si(111)$\sqrt{3} \times \sqrt{3}$-B and 7×7 substrates using scanning tunneling microscopy (STM) and Monte Carlo simulations. The value of θ_c was found to decrease with increasing growth rate on both substrates. At high growth rates, small Bi(110) islands were observed to nucleate at high density. These islands possessed rough edges that effectively trapped migrating Bi atoms, thereby suppressing Bi nucleation at the terraces of the preexisting Bi(110) islands and promoting the lateral extension of the islands. However, the interfacial strain cannot be relaxed by edges effectively in the laterally expanded Bi(110) island, causing θ_c to decrease with increasing growth rate.

II. METHODS

Experiments were conducted in an ultrahigh-vacuum (UHV) apparatus with a Bi Knudsen cell and an STM system [7,8]. The Si(111)$\sqrt{3} \times \sqrt{3}$-B substrates were prepared by flashing highly B-doped Si(111) samples at 1523 K for 25 s

*hirayama.h.aa@m.titech.ac.jp

 ©2022 American Physical Society

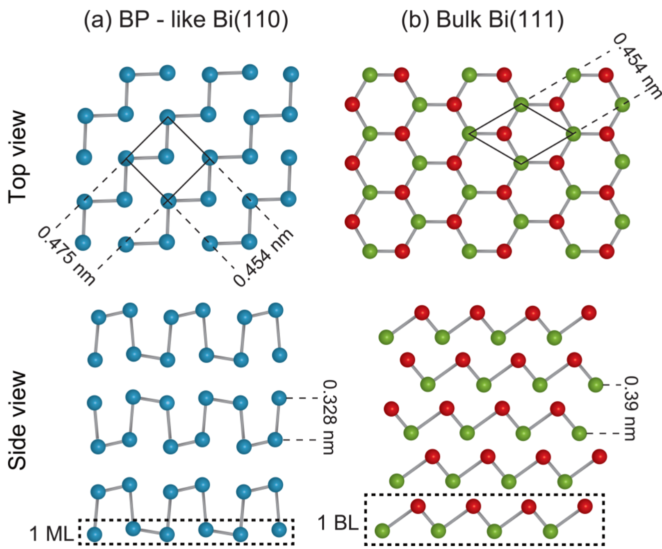

FIG. 1. Atomic arrangements of (a) Bi(110) islands with a BP-like structure and (b) Bi(111) islands with a rhombohedral structure. The Bi atoms arrange with a centered rectangular unit cell in the Bi(110) islands, whereas they arrange with a rhombic unit cell in the Bi(111) islands, as depicted in the top views.

and subsequent annealing at 1223 K for 30 min then 1173 K for 30 min. After annealing, the substrate was slowly cooled down to room temperature. The Si(111)7 × 7 substrates were also prepared by the thermal treatment of n-type Si(111) substrates in UHV. Bi atoms were deposited on the substrates at room temperature at various rates ranging from 0.035 to 0.60 ML/min. In this study, one ML was defined as the density of Bi atoms in a Bi(110) plane (9.27×10^{14} atoms/cm^2). The heights of the Bi islands were converted to ML units using the interlayer spacings of 0.328 nm for Bi(110) [8,20] and 0.390 nm for Bi(111) [22]. Since Bi islands start to nucleate after the Si substrate is covered by a wetting layer [20], the height of the Bi islands were measured from the wetting layer in STM. The nucleation and growth of the Bi islands and the arrangement of Bi atoms at the island surfaces were observed by STM at room temperature and liquid N_2 temperature. Details of the Monte Carlo simulations are described later.

III. RESULTS AND DISCUSSION

Figure 2 presents typical STM images showing the growth-rate dependence of the nucleation and growth of ultrathin Bi islands on the Si(111)$\sqrt{3} \times \sqrt{3}$-B substrate. The growth rate was 0.035 ML/min for the left column and 0.60 ML/min for the right column, and for each growth rate images were acquired for Bi coverages (θ) ranging from approximately 2 to 7 ML. All of the Bi islands were atomically flat, irrespective of the growth rate and θ. The atomic arrangements of the Bi islands are shown in the insets of Figs. 2(d), 2(g) and 2(h). Bi atoms arrange with a 0.454×0.475 nm^2 centered rectangular unit cell at BP-like Bi(110) surfaces, whereas they arrange in a hexagonal lattice with a 0.454×0.454 nm^2 rhombic unit cell at Bi(111) surfaces [3,8,20], as illustrated in Fig. 1. Thus the Bi islands in Figs. 2(a)–2(g) were assigned to BP-like Bi(110) islands, while those in Fig. 2(h) were identified as rhombohedral Bi(111) islands. These results indicate that the structural transition occurred during growth at a rate of 0.60 ML/min but not during growth at a rate of 0.035 ML/min in the θ range of up to approximately 7 ML.

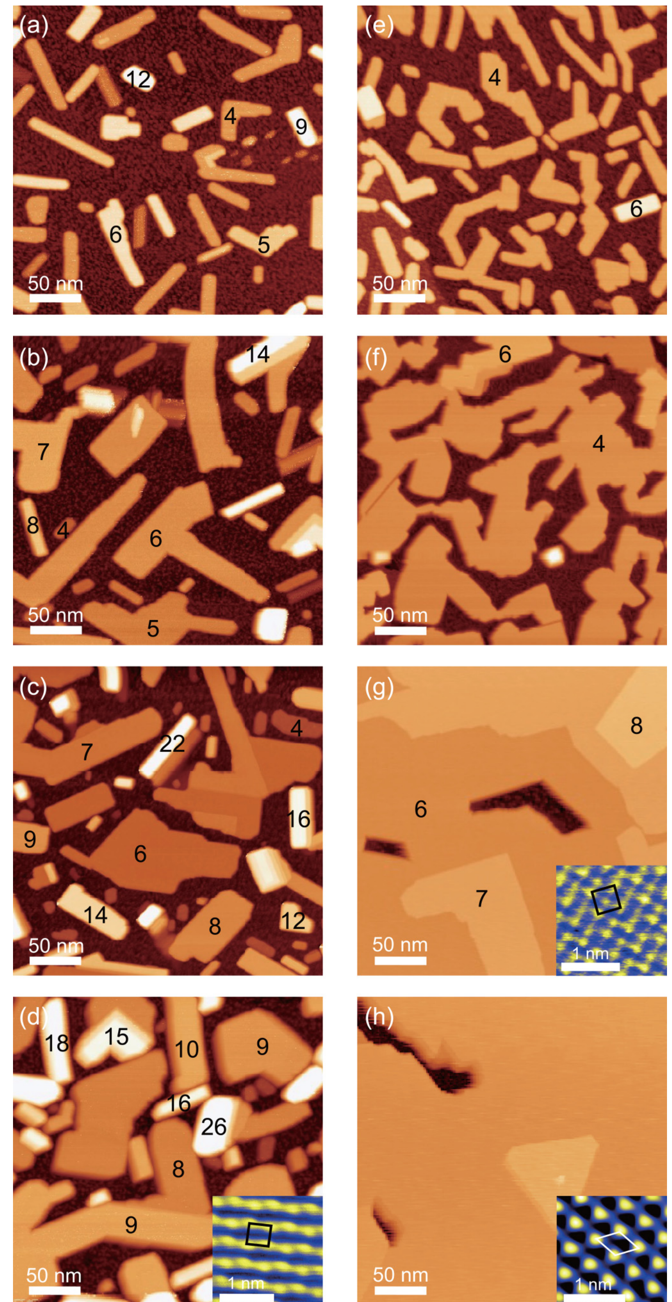

FIG. 2. STM images of the nucleation and growth of Bi islands on the Si(111)$\sqrt{3} \times \sqrt{3}$-B substrate at growth rates of (a)–(d) 0.035 ML/min and (e)–(h) 0.60 ML/min. The θ values are (a) 2.1 ML, (b) 3.8 ML, (c) 5.8 ML, (d) 7.3 ML, (e) 2.4 ML, (f) 4.0 ML, (g) 6.0 ML, and (h) 7.2 ML. The image size is 300×300 nm^2. The sample bias voltage (V_s) and tunneling current (I_t) were 2.0 V and 0.1 nA, respectively. The insets in (d), (g), and (h) show atomically resolved STM images of the Bi islands. The inset image size is 2×2 nm^2. The bias voltage and tunneling current were 0.04 V and 0.53 nA in (d), 0.23 V and 0.25 nA in (g), and 1.52 V and 0.1 nA in (h), respectively.

TABLE I. Growth-rate dependence of the critical thickness θ_c for the structural transition from Bi(110) to Bi(111). θ_c is given in units of Bi(110) ML.

Deposition rate (ML/min.)	0.035	0.040	0.045	0.11	0.13	0.18	0.47	0.6
Critical Thickness (ML) on Si(111)$\sqrt{3} \times \sqrt{3}$-B	>60	20	8	8	8	8	8	6
Critical Thickness (ML) on Si(111) 7×7	>15	–	–	–	–	10	9	8

During film growth at 0.035 ML/min, Bi(110) islands of various heights nucleated, as indicated in the figure in ML units for selected Bi(110) islands. The heights were distributed from 4 to 12 ML at $\theta = 2.1$ ML [Fig. 2(a)], from 4 to 14 ML at $\theta = 3.8$ ML [Fig. 2(b)], from 4 to 22 ML at $\theta = 5.8$ ML [Fig. 2(c)], and from 8 to 26 ML at $\theta = 7.3$ ML [Fig. 2(d)]. The islands were predominantly composed of even numbers of layers, as would be expected for BP-like Bi(110) islands. However, some islands were observed to contain odd numbers of layers. These Bi(110) islands were assigned to structures in which the lattice of the inner layers had temporarily changed to the rhombohedral structure as we reported in our previous study [8]. These are formed as a transient phase in the BL increase of the height of BP-structured Bi(110) islands. Although several Bi(110) islands with heights in excess of 16 ML were observed [Fig. 2(d)], the Bi(110) islands still remained at $\theta = 7.3$ ML during growth at 0.035 ML/min. In fact, the structural transition from BP-like Bi(110) to rhombohedral Bi(111) did not occur even at $\theta = 60$ ML during film growth at 0.035 ML/min on the Si(111)$\sqrt{3} \times \sqrt{3}$-B substrate. Although the transition could be induced by a post annealing at 700 K, the Bi(110) islands remained stably after the deposition of 60 ML Bi atoms with the rate of 0.035 ML/min at room temperature.

In contrast, most of the Bi(110) islands displayed a uniform height of 4 ML at $\theta = 2.4$ ML during film growth at 0.60 ML/min on the Si(111)$\sqrt{3} \times \sqrt{3}$-B substrate [Fig. 2(e)]. These Bi(110) islands exhibited a higher density compared with those observed at a growth rate of 0.035 ML/min. While the Bi(110) islands showed needle like shapes with straight edges in the growth at 0.035 ML/min, the edges included ledges and kinks to make the Bi(110) islands gnarled and tortuous in the growth at 0.60 ML/min as shown in Figs. 2(e) and 2(f). Upon further Bi deposition, the islands extended laterally while maintaining a height of 4 ML and coalesced with each other to form a continuous film [Fig. 2(f)], in contrast to the results observed at a growth rate of 0.035 ML/min where each island remained discrete and no continuous film was formed even at $\theta = 7.3$ ML. At $\theta = 6.0$ ML, the substrate was almost entirely covered by a Bi(110) film with a height of 6 ML [Fig. 2(g)]. Wide and flat terraces with heights of 7 or 8 ML were also present in some regions. The BP-like Bi(110) film had completely reorganized to a rhombohedral Bi(111) film everywhere by $\theta = 7.2$ ML [Fig. 2(h)]. In other words, the structural phase transition occurred at θ_c above 6 ML during film growth at 0.60 ML/min on the Si(111)$\sqrt{3} \times \sqrt{3}$-B substrate.

We conducted similar experiments to determine the values of θ_c on the Si(111)$\sqrt{3} \times \sqrt{3}$-B and 7×7 substrates at various growth rates. The results are summarized in Table I. Here, θ_c was defined as the coverage at which all the area completely reorganized to Bi(111). The reorganization was observed to occur all at once everywhere at a certain coverage on the Si(111)$\sqrt{3} \times \sqrt{3}$-B substrate as demonstrated in Fig. 2(h). However, small Bi(110) domains remained persistently on the Si(111)7×7 substrate even after the other area was transfered to the Bi(111) although most of all the area reorganized to Bi(111) on the Si(111)7×7 substrate. For example, all the Bi(110) area reorganized to the 6 BL high Bi(111) film at the Si(111)$\sqrt{3} \times \sqrt{3}$-B substrate at θ of 7.2 ML in the growth at 0.60 ML/min [Fig. 3(c)]. In the meantime, most of all the area reorganized to Bi(111) of the height of 4 ML, but several rectangular small Bi(110) domains still remained persistently on the Si(111)7×7 substrate at $\theta = 5.4$ and 6.0 ML in the growth at the same rate [Figs. 3(a) and 3(b)]. Due to the persistent small Bi(110) domains, θ_c on the Si(111)7×7 substrate became apparently larger than that on the Si(111)$\sqrt{3} \times \sqrt{3}$-B substrate although most of all the area on the Si(111)7×7 substrate reorganized to Bi(111) at a smaller height than on the Si(111)$\sqrt{3} \times \sqrt{3}$-B substrate in the growth at the rates of 0.18, 0.47 and 0.60 ML/min (Table I). However, θ_c on the Si(111)$\sqrt{3} \times \sqrt{3}$-B substrate was clearly larger than that on the Si(111)7×7 substrate at small rates. As shown in Figs. 2(d) and 2(h), the Bi(110) islands was observed to become smaller and isolated, and θ_c increased with the decrease of the growth rate on both the Si(111) $\sqrt{3} \times \sqrt{3}$-B and 7×7 substrates. The increase of θ_c was in particular prominent at the rates of 0.040 and 0.035 ML/min on the Si(111)$\sqrt{3} \times \sqrt{3}$-B substrate.

The growth-rate dependence of θ_c suggests that kinetic processes play important roles in the nucleation and growth of Bi films. The STM results revealed that increasing the growth rate led to high-density nucleation of small Bi(110) islands and their subsequent lateral extension to cover the substrate

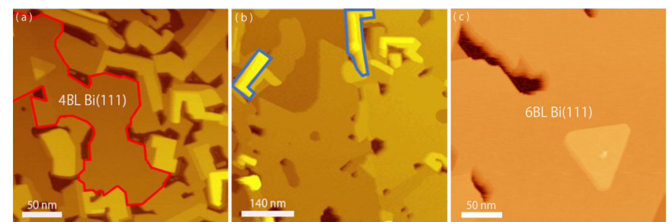

FIG. 3. STM images of the nucleation and growth of Bi islands on the Si(111)7×7 (a), (b) and $\sqrt{3} \times \sqrt{3}$-B substrate (c) at growth rates of 0.60 ML/min. θ was (a) 5.4, (b) 6.0, and (c) 7.2 ML. A locally rearranged Bi(111) area on the Si(111)7×7 substrate is surrounded by a red line in (a). Some of the persistently remained Bi(110) domains on the Si(111)7×7 substrate are highlighted by blue lines in (b). The image size is 300×300 nm^2 in (a) and (c), and 750×750 nm^2 in (b). The sample bias voltage (V_s) and tunneling current (I_t) were 2.0 V and 0.1 nA, respectively.

by a film of uniform height. The BP-like Bi(110) films reorganized to Bi(111) films at smaller values of θ_c as the growth rate was increased. However, the time resolution of STM is insufficient for following the underlying kinetic processes. Thus we performed Monte Carlo simulations to elucidate the influence of these kinetic processes on the nucleation and growth of Bi films.

The Monte Carlo simulations were conducted using the solid-on-solid model [23]. Bi atoms arranged in a centered rectangular lattice with a size of 0.475×0.454 nm in the BP-like Bi(110) plane were approximated by a square lattice with a size of 0.33 nm [$1/\sqrt{2}$ of (0.475+0.454)/2 nm]. The nucleation of the Bi(110) islands starts after the Si(111) substrate was covered by one ML thick Bi wetting layer. In this respect, we simulated the nucleation of the Bi(110) islands on the wetting layer. The Si(111) substrate with the threefold rotational symmetry was completely covered by the wetting layer. Bi atoms arrange aperiodically in the one ML thick wetting layer. However, it is practically impossible to grow the Bi(110) islands with the square lattice by the hopping of Bi atoms on randomly distributing sites in the simulation. Thus we adopted the square lattice with a size of 0.33 nm as a mimic of the wetting layer and made Bi atoms migrate on it. The kinetics of the Bi atoms are thought to be different on the wetting layer and at the top of the nucleated Bi(110) islands. Thus we prepared different parameters for the motion of the Bi atoms on the wetting layer and Bi(110) island in the simulation. In the simulation, we deposited Bi atoms on the mimic wetting layer. Since the wetting layer has one ML thickness, we injected $\theta - 1$ ML Bi atoms on the wetting layer in the simulation of the experimentally observed nucleation and growth process of θ ML Bi atoms. In each Monte Carlo step, the Bi atoms were made to perform a random walk on the square lattice [24] by hopping to one of the four nearest neighbor (NN) sites with a probability of 1/4. If a Bi atom found another atom at an NN site, it was bound to the site with a certain probability by reducing the hopping probability to the remaining NN sites by $exp(-E/kT)$. Here, E and k denote the activation energy and Boltzmann constant, respectively, and T was set to be 300 K. BP-like Bi(110) islands are composed of covalent ($E_{i,j}$) and noncovalent bonds ($E'_{i,j}$) in both the in-plane and out-of-plane directions, as depicted in Fig. 4, where the subscripts i, j indicate the numbers of the layers containing the two NN sites. To reflect the stronger binding of a Bi atom by a covalent bond than by a noncovalent bond, we set $E_{i,i+1} \geqslant E'_{i+1,i+2}$ along the surface normal orientation and $E_{i,i} \geqslant E'_{i,i}$ in the same plane. The bottom bilayer grows directly on the wetting layer while the upper layers grow on previously deposited Bi layers. Thus we set $E_{i,i}$ and $E'_{i,i}$ for i=1 and 2 different from those in the upper layers to reflect the difference in the kinetics of the Bi atoms on the wetting layer and on the Bi(110) islands. Furthermore, it has been demonstrated experimentally that BP-like Bi(110) islands with a height of 4 ML are preferentially formed during the initial stage of film growth [7,8,22]. This preference was reflected in the simulations by making $E'_{2,3}$ larger than $E'_{i+1,i+2}$ for the upper layers. If a Bi atom was surrounded by multiple atoms at NN sites, the hopping was further restricted by replacing the activation energy with the sum of the $E_{i,j}$ values for each bond.

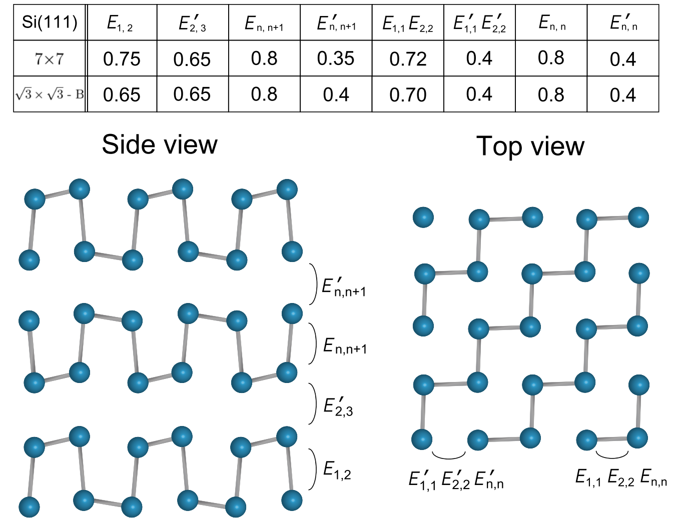

Si(111)	$E_{1,2}$	$E'_{2,3}$	$E_{n,n+1}$	$E'_{n,n+1}$	$E_{1,1}$ $E_{2,2}$	$E'_{1,1}$ $E'_{2,2}$	$E_{n,n}$	$E'_{n,n}$
7×7	0.75	0.65	0.8	0.35	0.72	0.4	0.8	0.4
$\sqrt{3} \times \sqrt{3}$ - B	0.65	0.65	0.8	0.4	0.70	0.4	0.8	0.4

FIG. 4. Parameters used in the Monte Carlo simulations on the Si(111)7 × 7 and Si(111)$\sqrt{3} \times \sqrt{3}$-B substrates. E is given in units of eV.

The adsorption energy of Bi atom to the wetting layer E_{01} was taken implicitly via. the time interval of the hopping of Bi atom $\tau = (1/\nu_0)\exp(E_{01}/kT)$ in the simulation. Here, ν_0 is the attempt frequency. The Bi atom on the square lattice hops at each MC step, while a new Bi atom is injected every 70 and 300 MC steps into the area of 150×150 nm^2 in the simulation of the growth at 0.035 ML/min on the Si(111)7 × 7 and $\sqrt{3} \times \sqrt{3}$-B substrate, respectively. From the number of MC steps between the Bi atom injections, one MC step ($=\tau$) is evaluated to correspond to 1.2×10^{-4} and 2.8×10^{-5} sec on theses substrates. These τs are reproduced by $E_{01} = 0.54$ and 0.51eV, respectively with a conventional attempt frequency ν_0 of 10^{13} Hz at $T = 300$ K. Bi atom hops on the substrate (= wetting layer) with these adsorption energy E_{01} in the simulation on the Si(111)7 × 7 and $\sqrt{3} \times \sqrt{3}$-B substrates. When the migrating Bi atom encounters the other Bi atom, they make bond to form a nucleus. The stability of the nucleus is expressed by reducing the hopping probability by a factor of $exp(-E_{ij}/kT)$ in the simulation. It means that the activation barrier for the hopping becomes $E + E_{ij}$ for the aggregated Bi atom. The re-evaporation of Bi atoms was neglected in the simulations because this process does not happen at room temperature. The Ehrlich-Schwoebel [25,26] barrier was also neglected for simplicity.

The $E_{i,j}$ and $E'_{i,j}$ values were selected to reproduce the experimentally observed characteristics of the nucleation and growth of Bi(110) islands on the Si(111)7 × 7 and Si(111)$\sqrt{3} \times \sqrt{3}$-B substrates by STM. The adopted values are listed in Fig. 4. Figure 5 demonstrates the consistency between the simulation and STM results during film growth on the Si(111)7 × 7 and $\sqrt{3} \times \sqrt{3}$-B substrate at a rate of 0.035 ML/min. The nucleated Bi(110) islands oriented randomly in plane on the Si(111)7 × 7 substrate [3], while they preferred to extend along six specific orientations on the Si(111)$\sqrt{3} \times \sqrt{3}$-B substrate due to the Bi(110) and Si(111)$\sqrt{3} \times \sqrt{3}$ lattice commensuration at the interface [7]. The preference of the specific orientations on the Si(111)$\sqrt{3} \times \sqrt{3}$-B substrate

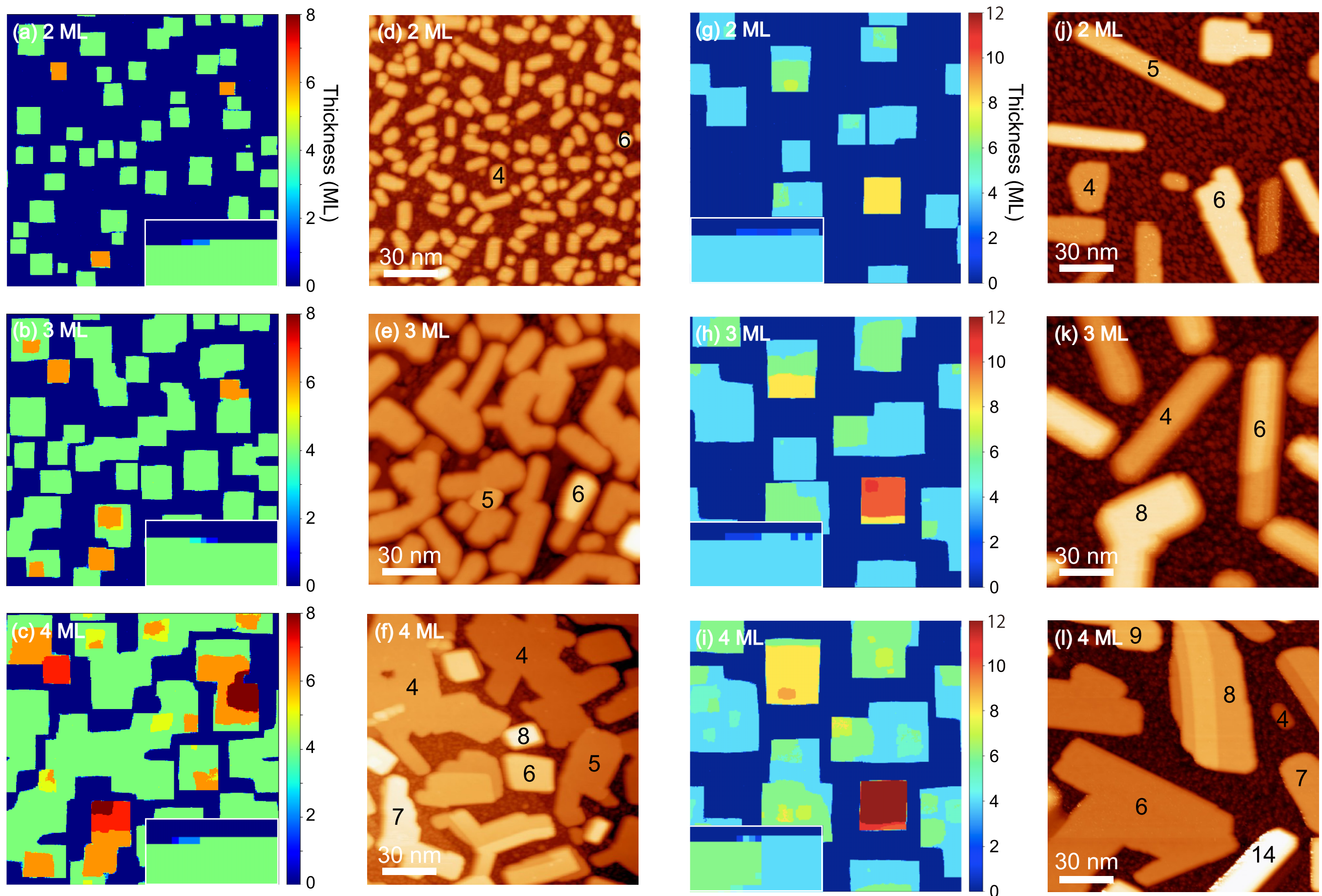

FIG. 5. Comparison of Monte Carlo simulation snapshots and STM images during film growth at 0.035 ML/min on the Si(111)7 × 7 [(a)–(f)] and Si(111)$\sqrt{3} \times \sqrt{3}$-B [(g)–(l)] substrates. Monte Carlo simulation snapshots are displayed in (a)–(c) and (g)–(i), while STM images are displayed in (d)–(f) and (j)–(l), respectively. The image size is 150 × 150 nm^2 in all cases. The Bi coverage θ is 2 ML in (a), (d), (g), and (j); 3 ML in (b), (e), (h), and (k); and 4 ML in (c), (f), (i), and (l). The zoomed-in insets in (a)–(c) and (g)–(i) show the typical shapes of the island edges from the simulations. The STM images were recorded at a bias voltage and tunneling current of 2.0 V and 0.1 nA, respectively.

is not possible to be taken into the simulation with the sites on the fourfold square lattice. However, except for this point, the experimental results were well reproduced by the simulations. We also performed simulations of other growth rates by assuming a linear relation between the injection rate and growth rate. Figure 6 presents simulation snapshots at $\theta = 2$, 3, and 4 ML for growth rates of 0.18 and 0.60 ML/min. This series of simulations at 0.035 ML/min (Fig. 5) and 0.18 and 0.60 ML/min (Fig. 6) satisfactorily reproduced the experimentally observed trend that the island density increases with increasing growth rate. Furthermore, the simulations successfully reproduced the experimental observations of the Bi(110) islands remaining isolated with various heights at low growth rates and maintaining a constant height of 4 ML and extending laterally at high growth rates in the later stages of film growth on both the Si(111)7 × 7 and $\sqrt{3} \times \sqrt{3}$-B substrates.

The kinetics of the initial island nucleation was theoretically revealed to be governed by the parameter $\Gamma = D/F$, where D is the diffusion constant and F is the deposition flux rate in the analysis of rate equations [27–29]. The island density at coverage θ can be expressed analytically as $n(\Gamma, \theta) \propto \Gamma^{-\chi}$, where χ is positive [29,30]. In fact, the density of nucleated islands has been experimentally observed to increase with decreasing D by lowering T in such diverse systems as $C_{60}/CaF_2(111)$, Au/Au(110), and Fe/Fe(100) [31–33]. In a comparison of Figs. 2(a) and 5(d) ($\theta = 2$ ML, the rate was 0.035 ML/min.), it is noticed that the Bi(110) islands nucleated more densely on the Si(111)7 × 7 substrate than on the Si(111)$\sqrt{3} \times \sqrt{3}$-B substrate at the initial stage. We regard that it was also caused by the difference of D on these substrates. The surface dangling bonds are fully passivated on the Si(111)$\sqrt{3} \times \sqrt{3}$-B substrate but not on the Si(111)7 × 7 substrate [7]. Thus D of the Bi atom on the Si(111)7 × 7 substrate is expected to be smaller than that on the Si(111)$\sqrt{3} \times \sqrt{3}$-B substrate to cause the more densely nucleation of the islands.

The initially nucleated Bi(110) islands extend laterally while maintaining a constant height of 4 ML to form a continuous film of uniform height during film growth at a high rate on both the Si(111)7 × 7 and $\sqrt{3} \times \sqrt{3}$-B substrates. One of the characteristics of film growth at a high rate is the high-density nucleation of Bi(110) islands in the initial stage. In this work, D was kept constant at $T = 300$ K while F was increased in contrast to the previous studies in which Γ decreased with decreasing D under constant F. However, this also led to a decrease in Γ. In this respect, the high-density nucleation of Bi(110) islands at high growth rates is

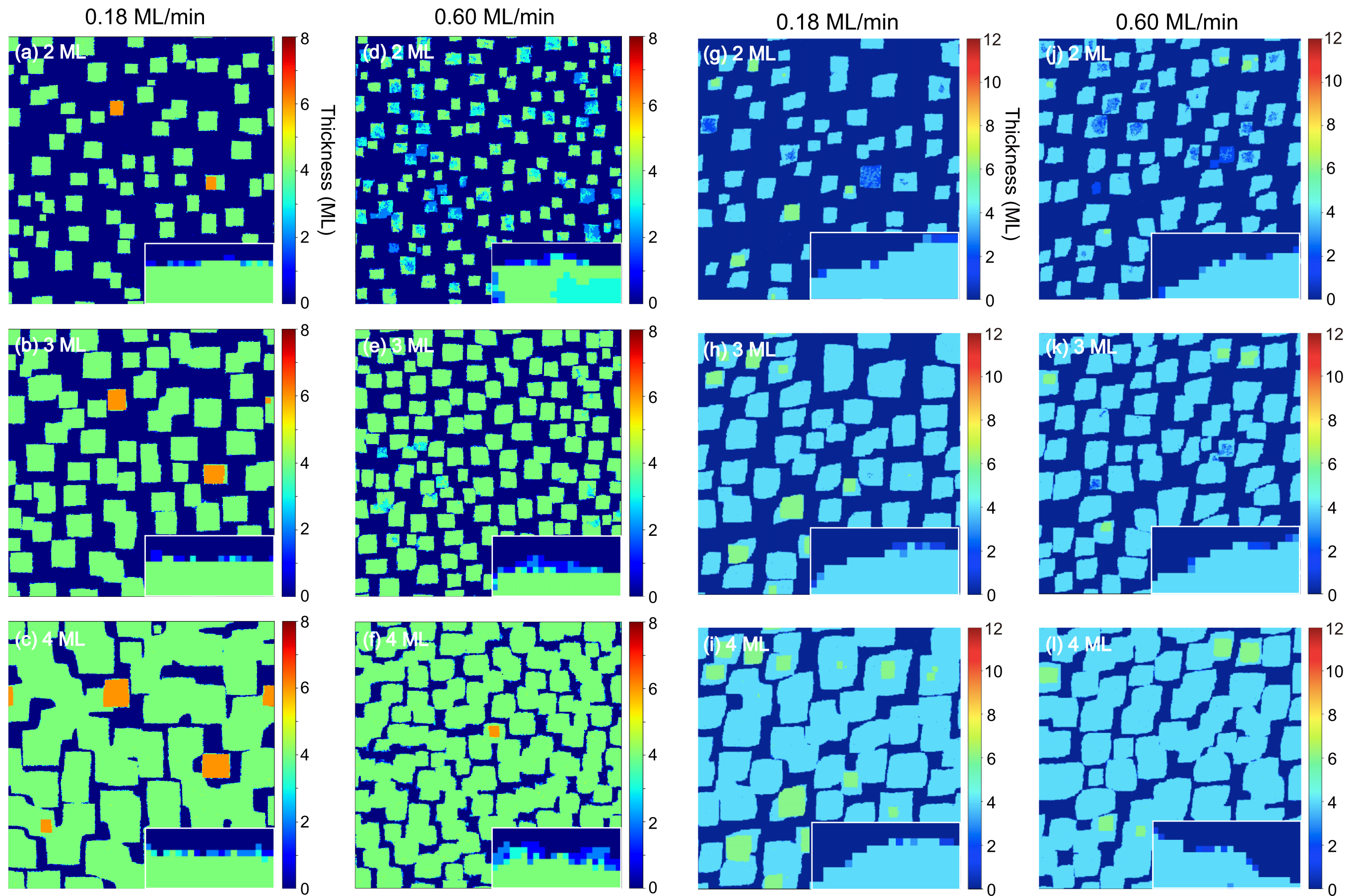

FIG. 6. Monte Carlo simulation snapshots showing the nucleation and growth of Bi islands during film growth on the Si(111)7 × 7 [(a)–(f)] and Si(111)$\sqrt{3} \times \sqrt{3}$-B [(g)–(l)] substrates at 0.18 ML/min and 0.60 ML/min. [(a)–(c) and (g)–(i)] 0.18 ML/min and [(d)–(f) and (j)–(l)] 0.60 ML/min. The image size is 150 × 150 nm^2 in all cases. The Bi coverage θ is 2 ML in (a), (d), (g), and (j); 3 ML in (b), (e), (h), and (k); and 4 ML in (c), (f), (i), and (l). The zoomed-in insets show the typical shapes of the island edges in the simulations.

reasonable. The number of migrating Bi atoms increases with the impinging rate of Bi atoms F. The impinged Bi atoms migrate on the substrate randomly and form stable nuclei if they encounter each other during migration. The nucleation rate is approximately proportional to the square of the number of migrating atoms. Therefore a higher deposition rate leads to a faster increase in the number of migrating Bi atoms on the substrate. Thus the density of islands increases with the growth rate in the present case.

Once the Bi(110) islands have become established in the initial stage ($\theta \leqslant 2$ ML), they serve as sinks for the migrating atoms [21]. Migrating atoms encounter the preexisting islands with much higher probability than they encounter the other randomly walking atoms. Thus most of the migrating atoms are adsorbed onto the preexisting islands and the nucleation of new islands in the gaps between the preexisting islands hardly occurs. In fact, no increase in the number of Bi(110) islands was observed at θ values above 2 ML in either the STM experiments or the simulations. The Bi(110) islands extend laterally by adsorbing the migrating atoms. Here, the islands would grow dendritically if the edges could never release the attached Bi atoms. Actually, such a dendritic nucleation occurred in a simulation in which E_{ii} and E'_{ii} were deliberately set to be 1.5 eV to make the bonding energies to the edges larger than those in the table in Fig. 4. However, the Bi atoms at the edge of the islands were able to be released and hop in the simulation with E_{ii} and E'_{ii} in Fig. 4 since the simulation with these E_{ii} and E'_{ii} reproduced the experimentally observed nucleation and growth of the Bi(110) islands and its rate-dependence as demonstrated in Figs. 5 and 6.

Injected Bi atoms land not only in the gaps between the islands but also on top of the islands in a certain increasing ratio as the islands continue to laterally expand. Thus the injected atoms randomly walk on both the islands and the exposed wetting layer in the gap regions. If the migrating atoms frequently encounter each other on the Bi(110) islands, higher terraces can nucleate on the Bi(110) islands to afford an inhomogeneous height distribution. Meanwhile, the Bi(110) islands further extend laterally while maintaining a constant height if the randomly walking atoms preferentially attach at the edges of the islands during the course of their migration. We consider that the former case occurred during film growth at lower rates, whereas the latter case occurred during film growth at higher rates.

A key to distinguishing between these two cases is the preference for attachment of the migrating atoms at the island edges. The insets in Figs. 5 and 6 show zoomed-in snapshot images of the island edges from the simulations. These images reveal that the island edges were relatively straight during film growth at a low rate but rough and with

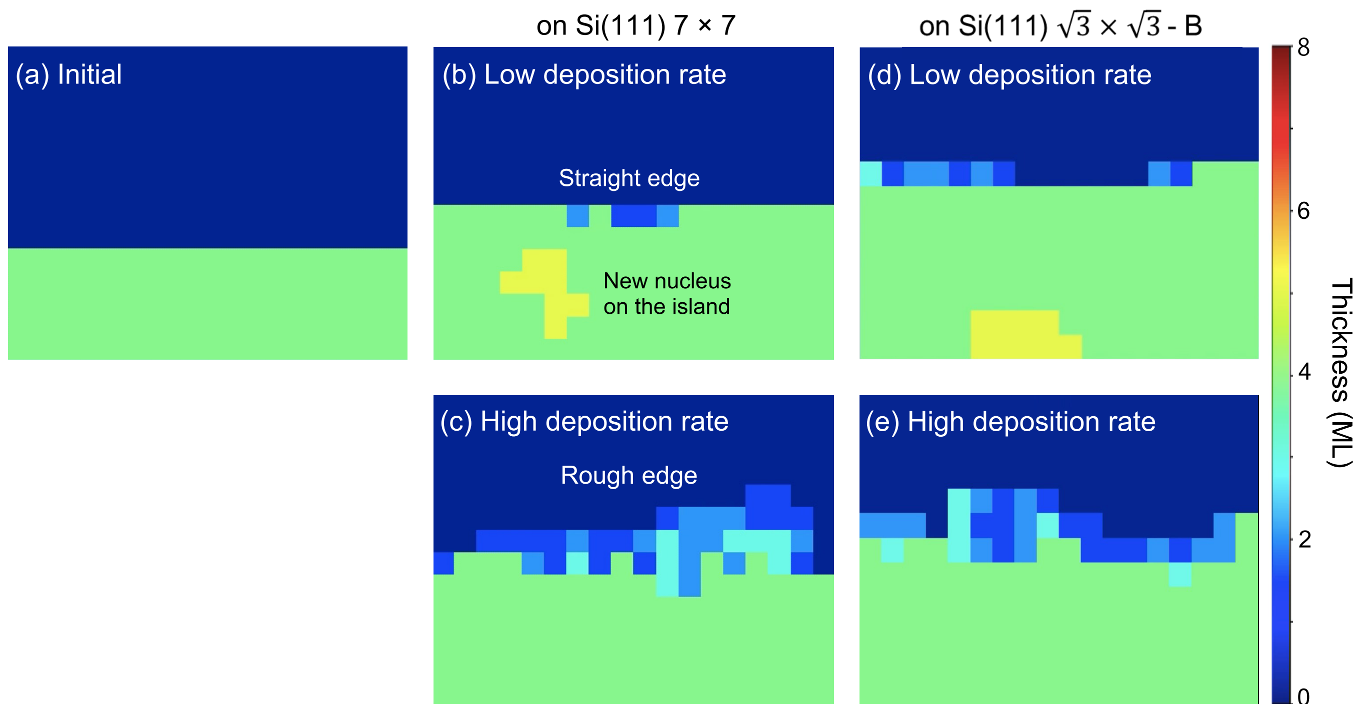

FIG. 7. Monte Carlo simulation snapshots showing the effects of the growth rate on the edge shape and nucleation on the Bi(110) islands on the Si(111)7 × 7 and Si(111)$\sqrt{3} \times \sqrt{3}$-B substrates. (a) A 4 ML thick Bi(110) island is prepared in the bottom half of the area of 74 × 74 nm^2. (b) and (c) are the results after depositing 0.4 ML of Bi atoms on the Si(111)7 × 7 substrate at growth rates of 0.035 and 0.60 ML/min, respectively. (d) and (e) are the results after depositing 0.4 ML of Bi atoms on the Si(111)$\sqrt{3} \times \sqrt{3}$-B substrate at growth rates of 0.035 and 0.60 ML/min, respectively.

numerous kinks during growth at a high rate. Actually, such a change of the island edge was experimentally observed in STM (Fig. 2). Because migrating atoms can be bound at the kink sites by many bonds, they are trapped much more efficiently at rough edges than at straight edges. We consider that this accounts for the lateral extension of the Bi(110) islands without the nucleation of higher terraces on their upper surfaces during film growth at high rates. Because migrating atoms are trapped less efficiently at straight edges, they have greater opportunity to encounter one another on the tops of preexisting islands to form higher terraces and afford an inhomogeneous height distribution during film growth at low rates.

The edges of the Bi(110) islands are considered to become rough at high growth rates through the following mechanism. The random attachment of migrating atoms to an island results in the formation of rough edges. Each attached atom preferentially migrates along the edge rather than dissociating into the free space [34,35] because it finds more bonding counterparts at the island edge. Kink sites in particular are energetically preferable at the island edge. Accordingly, the attached Bi atom migrates until it finds and fills a kink to make the edge straight if it has sufficient time to attempt many hopping steps along the island edge. However, if a large number of atoms are injected in a short interval, a second atom can attach to the island edge before the first attached atom fills a kink site. This leads to Bi(110) islands with rough edges during film growth at high rates.

The islands are able to adopt their thermal equilibrium structures if the interval is sufficiently long, but this is not the case under the short interval in the above context. In the simulations, Bi(110) islands with a stable height of 4 ML appeared from the beginning of nucleation at a low growth rate [Figs. 5(a) and 5(g)], but a considerable number of the islands possessed a height of 2 ML at a high growth rate [Figs. 6(d) and 6(j)]. This is also considered to be attributable to the relatively short interval for Bi atom injection during film growth at a high rate.

We performed further simulations to verify that the Bi atoms make the island edges rough and suppress terrace nucleation on the islands at high growth rates. For this purpose, we prepared a 4-ML-thick Bi(110) island with a straight edge in the lower half of the 74 × 74 nm^2 area on the Si(111)7 × 7 and $\sqrt{3} \times \sqrt{3}$-B substrates as shown in Fig. 7(a). Bi atoms were then randomly injected into the simulation area at rates of 0.035 and 0.60 ML/min. Figures 7(b) and 7(c) present the results after the deposition of 0.4 ML of Bi atoms on the Si(111)7 × 7 substrate. The results on the Si(111)$\sqrt{3} \times \sqrt{3}$-B substrate are shown in Figs. 7(d) and 7(e). Although the Bi atoms were injected evenly on the 4-ML-thick Bi(110) island and the uncovered substrate, no nucleation of higher terraces was observed on the Bi(110) island during growth at 0.60 ML/min. The edge clearly became rough and all of the injected Bi atoms were adsorbed at this rough edge. In contrast, a higher terrace nucleated on the Bi(110) island during growth at 0.035 ML/min. The edge retained its straight shape although it had laterally extended after the deposition. These results support the mechanisms discussed above.

How is the rate-dependent change of the nucleation and growth of the Bi(110) islands related to the critical thickness

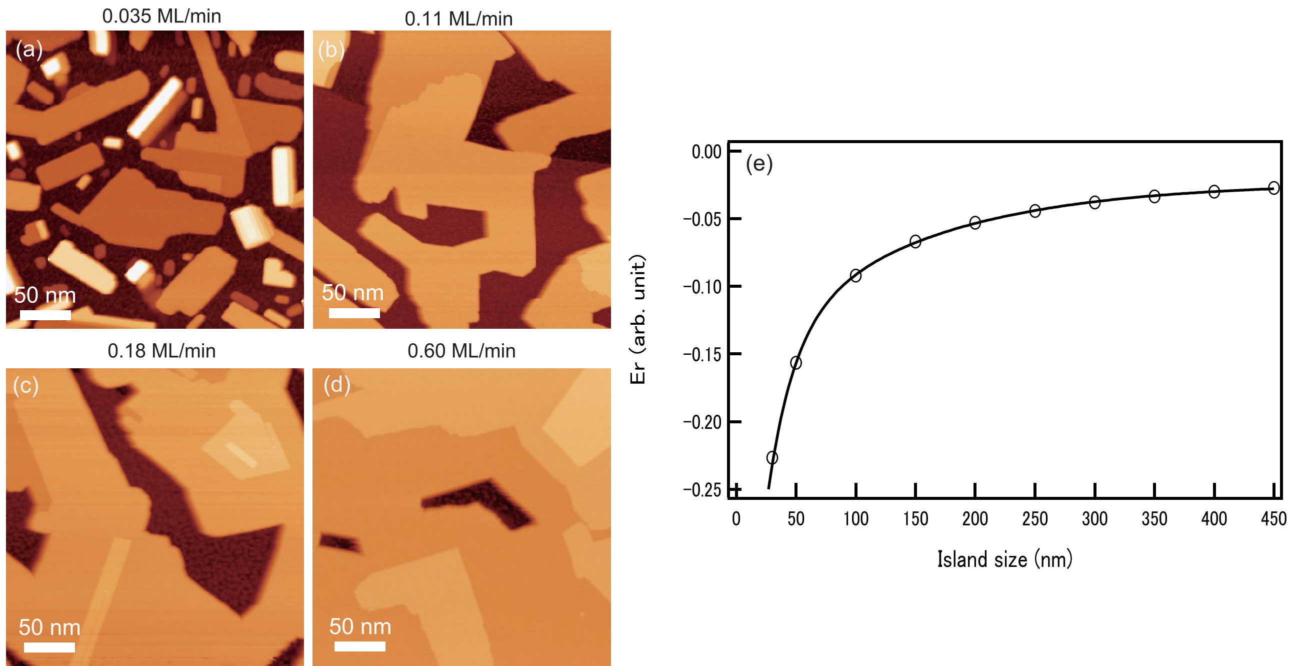

FIG. 8. The growth rate-dependence of the size of the Bi(110) islands on the Si(111)$\sqrt{3}\times\sqrt{3}$-B substrate. [(a)–(d)] STM images at $\theta = 6$ ML for 0.035, 0.11, 0.18, and 0.60 ML/min. $V_s = 2.0$ V. $I_t = 0.1$ nA. 300×300 nm^2. (e) The island size dependent change of the strain energy relaxation per area in the analytical equation [36].

for the transition to the Bi(111) structure? We consider that the key is the in-plane area of the Bi(110) islands. In the BP-like structure, the Bi atoms must adopt a buckled arrangement to construct the paired layer, leading to the accumulation of strain energy in the (110) plane. In addition, the lattice mismatch at the interface also introduces strain into the Bi(110) islands. However, the strain energy is relaxed at the edges of the island [36–38]. Thus a small Bi(110) island can relax the strain energy more efficiently than a large Bi(110) island. Since the Bi(110) island with a smaller strain energy has a lower merit to rearrange to the Bi(111) structure, it keeps the BP-like (110) structure even at larger heights. We consider that this is the reason why θ_c increases in the growth of lower rate with the nucleation of small Bi(110) islands.

The strain energy per area is theoretically described as $E_r \propto -(1/t)ln(t) - (1/s)ln(s) + \alpha$ for the island with the length s and width t [36]. α is a constant independent of s and t. For simplicity, we assume $s = t$ and $\alpha = 0$ and evaluated E_r as a function of the island size s in Fig. 8(e). E_r decreases gradually with the decrease of the island size for relatively large islands while it decreases steeply for small islands. We consider that this island size dependence of E_r is the immediate cause of the rate-dependent change of θ_c in Table I. Figures 8(a)–8(d) show STM images of the rate-dependent change of the Bi(110) island size at $\theta = 6$ ML on the Si(111)$\sqrt{3}\times\sqrt{3}$-B substrate. The size of the Bi(110) island decreased gently in the range of hundreds nm with the decrease of the growth rate from 0.60 to 0.11 ML/min, while it decreased steeply into the range of tens nm at 0.035 ML/min. Thus, with the decrease of the growth rate, the strain in the Bi(110) island decreases gradually at a rate above 0.11 ML, but is reduced drastically at smaller rates. It is consistent with the gradual increase of θ_c for rates above 0.045 ML/min and the steep jump for rates below 0.040 ML/min with the decrease of the growth rate.

θ_c on the Si(111)$\sqrt{3}\times\sqrt{3}$-B substrate was larger than that on the Si(111)7×7 substrate at small rates. In addition, most of the Bi(110) islands on the Si(111)7×7 substrate also reorganized to the Bi(111) islands at a smaller height than those on the Si(111)$\sqrt{3}\times\sqrt{3}$-B substrate at large rates, although θ_c on the Si(111)7×7 substrate was apparently larger than that on the Si(111)$\sqrt{3}\times\sqrt{3}$-B substrate due to the persistently remaining small Bi(110) domains. These means that the Bi(110) island on the Si(111)$\sqrt{3}\times\sqrt{3}$-B substrate is more persistent against the structural transition than that on the Si(111)7×7 substrate. We regard that this is due to the difference in the stacking of the Bi(110) lattice at the interface. The Bi(110) islands preferentially grow so as to align the diagonal of the unit cell along the $\{1\bar{1}0\}$ orientation at the Si(111)$\sqrt{3}\times\sqrt{3}$-B substrate [7] because the 0.475×0.454 nm^2 centered rectangular unit cell of the Bi(110) plane becomes commensurate with the 0.665×0.665 nm^2 rhombic unit cell of Si(111)$\sqrt{3}\times\sqrt{3}$-B substrate at a ratio of 7:4 along the $\{1\bar{1}0\}$ orientation, as illustrated in Fig. 9(a). In contrast, Bi(110) islands were oriented randomly on the Si(111)7×7 substrate to show a ring-like pattern in low-energy electron diffraction [3]. This suggests that Bi(110) islands are bound more weakly on the Si(111)7×7 substrate than on the Si(111)$\sqrt{3}\times\sqrt{3}$-B substrate. Upon the structural transition to Bi(111), the bonds at the interface layer are necessary to be rearranged. Thus the transition of the commensurate Bi(110) islands will need more energy in the structural transition. We consider that this is the reason why the transition on the Si(111)$\sqrt{3}\times\sqrt{3}$-B substrate occurred at a larger θ_c than on the Si(111)7×7 substrate generally. An exception is the persistently remaining Bi(110) domains on the Si(111)7×7 substrate which oriented to the same di-

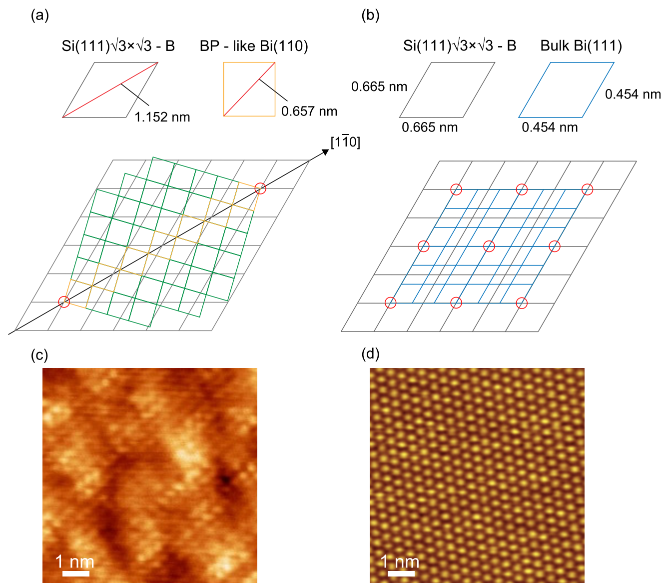

FIG. 9. Lattice commensuration of (a) the Bi(110) plane with a rectangular unit cell and (b) the Bi(111) plane with a rhombic unit cell to the Si(111)$\sqrt{3} \times \sqrt{3}$-B substrate with a rhombic unit cell. Atomically resolved STM images of the (c) Bi(110) and (d) Bi(111) islands. The image size is 8×8 nm^2. V_s and I_t were −0.5 V and 0.3 nA in (c) and 1.3 V and 0.1 nA in (d), respectively.

rection of the Bi(110) islands on the Si(111)$\sqrt{3} \times \sqrt{3}$-B substrate. Their persistence against the structural transition seems to be also due to the commensuration of the diagonal of the Bi(110) lattice along the Si(111) {1$\bar{1}$0} orientation, although the commensuration along the direction is thought not so satisfactorily on the 7×7 reconstructed substrate. The persistent Bi(110) domains on the Si(111)7×7 substrate were small enough and are expected to release the strain effectively. In contrast, the size of the Bi(110) islands on the Si(111)$\sqrt{3} \times \sqrt{3}$-B substrate was much larger than that of the persistently remaining Bi(110) domains on the Si(111)7×7 substrate at large growth rates as shown in Figs. 3(a)–3(c), respectively. Thus θ_c is considered to become apparently larger on the Si(111)7×7 substrate than on the Si(111)$\sqrt{3} \times \sqrt{3}$-B substrate at large rates. However, the size of the fully commensurate Bi(110) islands became small enough at low growth rates even on the Si(111)$\sqrt{3} \times \sqrt{3}$-B substrate as shown in Fig. 2(d). We regard that this is the reason why θ_c on the Si(111)$\sqrt{3} \times \sqrt{3}$-B substrate became larger than that on the Si(111)7×7 substrate at small rates.

IV. SUMMARY

In summary, we have investigated the growth-rate dependence of the nucleation, growth, and structural transition of Bi islands on the Si(111)$\sqrt{3} \times \sqrt{3}$-B and 7×7 substrates using STM and Monte Carlo simulations. Bi(110) islands of various heights were observed to nucleate separately during film growth at low rates. In contrast, at high growth rates, Bi(110) islands with a height of 4 ML preferentially nucleated and then extended laterally to coalesce and afford a wide continuous film of uniform height. The value of θ_c for the structural transition from Bi(110) to Bi(111) decreased with increasing growth rate. The edges of the Bi(110) islands were found to be straight at low growth rates but rough with numerous kink sites at high growth rates in the simulations. The rough edges containing kink sites can efficiently trap migrating atoms, thus suppressing the nucleation of higher terraces on preexisting Bi(110) islands and promoting the lateral extension of the islands. Thus the widely extended Bi(110) film with uniform height was obtained at large growth rates while the small Bi(110) islands with various heights nucleated at low growth rates. In the meantime, the strain is released efficiently at the edges of small islands but not at the edges of the laterally extended wide islands. Therefore the structural transition occurred at small θ_cs at large growth rates but θ_c increased with the decrease of the size of the Bi(110) islands at low growth rates.

ACKNOWLEDGMENTS

We thank Taiga Kasai and Naoki Sasagawa for their assistance in the height analysis of Bi islands in STM images.

[1] S. Murakami, Phys. Rev. Lett. **97**, 236805 (2006).

[2] Y. Lu, W. Xu, M. Zeng, G. Yao, L. Shen, M. Yang, Z. Luo, F. Pan, K. Wu, T. Das, P. He, J. Jiang, J. Martin, Y. P. Feng, H. Lin, and X. Wang, Nano Lett. **15**, 80 (2015).

[3] T. Nagao, J. T. Sadowski, M. Saito, S. Yaginuma, Y. Fujikawa, T. Kogure, T. Ohno, Y. Hasegawa, S. Hasegawa, and T. Sakurai, Phys. Rev. Lett. **93**, 105501 (2004).

[4] G. Bian, T. Miller, and T.-C. Chiang, Phys. Rev. B **80**, 245407 (2009).

[5] S. Yaginuma, K. Nagaoka, T. Nagao, G. Bihlmayer, Yu. M. Koroteev, E. V. Chulkov, and T. Nakayama, J. Phys. Soc. Jpn. **77**, 014701 (2008).

[6] J. T. Sadowski, T. Nagao, S. Yaginuma, Y. Fujikawa, T. Sakurai, A. Oreshkin, M. Saito, and T. Ohno, J. Appl. Phys. **99**, 014904 (2006).

[7] I. Kokubo, Y. Yoshiike, K. Nakatsuji, and H. Hirayama, Phys. Rev. B **91**, 075429 (2015).

[8] K. Nagase, I. Kokubo, S. Yamazaki, K. Nakatsuji, and H. Hirayama, Phys. Rev. B **97**, 195418 (2018).

[9] S. Yaginuma, T. Nagao, J. T. Sadowski, M. Saito, K. Nagaoka, Y. Fujikawa, T. Sakurai, and T. Nakayama, Surf. Sci. **601**, 3593 (2007).

[10] D. Lükermann, S. Banyoudeh, C. Brand, S. Sologub, H. Pfnür, and C. Tegenkamp, Surf. Sci. **621**, 82 (2014).

[11] S. Hatta, Y. Ohtsubo, A. Miyamoto, H. Okuyama, and T. Aruga, Appl. Surf. Sci. **256**, 1252 (2009).

[12] C. Koitzsch, M. Bovet, F. Clerc, D. Naumovic, I. Schlapbach, and P. Aebi, Surf. Sci. **527**, 51 (2003).

[13] S. A. Scott, M. V. Kral, and S. A. Brown, Surf. Sci. **587**, 175 (2005).

[14] P. J. Kowalczyk, O. Mahapatra, S. A. Brown, G. Bian, X. Wang, and T.-C. Chiang, Nano Lett. **13**, 43 (2013).
[15] P. J. Kowalczyk, O. Mahapatra, D. N. McCarthy, W. Kozlowski, Z. Klusek, and S. A. Brown, Surf. Sci. **605**, 659 (2011).
[16] P. J. Kowalczyk, D. Belic, O. Mahapatra, S. A. Brown, E. S. Kadantsev, T. K. Woo, B. Lagham, and W. Kozlowski, Appl. Phys. Lett. **100**, 151904 (2012).
[17] J.-T. Sun, H. Huang, S. L. Wong, H.-J. Gao, Y. P. Feng, and A. T. S. Wee, Phys. Rev. Lett. **109**, 246804 (2012).
[18] L. Peng, J.-J. Xian, P. Tang, A. Rubio, S.-C. Zhang, W. Zhang, and Y.-S. Fu, Phys. Rev. B **98**, 245108 (2018).
[19] H. R. Sharma, V. Fournée, M. Shimoda, A. R. Ross, T. A. Lograsso, P. Gille, and A. P. Tsai, Phys. Rev. B **78**, 155416 (2008).
[20] H. Hirayama, Adv. Phys. X **6**, 1845975 (2020).
[21] Y. Saito, *Statistical Physics of Crystal Growth* (World Scientific, Singapore, 1996).
[22] K. Nagase, R. Ushioda, K. Nakatsuji, T. Shirasawa, and H. Hirayama, Appl. Phys. Express **13**, 085506 (2020).
[23] C. I. Fornari, G. Fornari, P. H. de O. Rappl, E. A. Bramof, J. dos S. Travelho, Monte Carlo simulation of Epitaxial Growth, http://dx.doi.org/10.5772/intechopen.70220 (2018).
[24] A. Zangwill, *Physics of Surfaces* (Cambridge University Press, Cambridge, 1988).
[25] R. L. Schwoebel, J. Appl. Phys. **37**, 3682 (1966).
[26] G. Ehrlich and F. G. Hidda, J. Chem. Phys. **44**, 1039 (1966).
[27] H. Brune, Surf. Sci. Rep. **31**, 125 (1998).
[28] J. W. Evans, P. A. Thiel, and M. C. Bartelt, Surf. Sci. Rep. **61**, 1 (2006).
[29] M. Einax, W. Dieterich, and P. Maass, Rev. Mod. Phys. **85**, 921 (2013).
[30] W. Dieterich, M. Einax, and P. Maass, Eur. Phys. J. Spec. Top. **161**, 151 (2008).
[31] F. Loske, J. Lübbe, J. Schütte, M. Reichling, and A. Kühnle, Phys. Rev. B **82**, 155428 (2010).
[32] S. Günther, E. Kopatzki, M. C. Bartelt, J. W. Evans, and R. J. Behm, Phys. Rev. Lett. **73**, 553 (1994).
[33] J. A. Stroscio and D. T. Pierce, Phys. Rev. B **49**, 8522 (1994).
[34] S. Schinzer, M. Kinne, M. Biehl, and W. Kinzel, Surf. Sci. **439**, 191 (1999).
[35] J. G. Amar, Phys. Rev. B **60**, R11317(R) (1999).
[36] J. Tersoff and R. M. Tromp, Phys. Rev. Lett. **70**, 2782 (1993).
[37] B. Müller, L. P. Nedelmann, B. Fischer, H. Brune, J. V. Barth, K. Kern, D. Erdös, and J. Wollschläger, Surf. Rev. Lett. **05**, 769 (1998).
[38] H. J. W. Zandvliet and R. van Gastel, Phys. Rev. Lett. **99**, 136103 (2007).